RSC Advances

ROYAL SOCIETY OF CHEMISTRY

www.rsc.org/advances

Highly Reversible Lithium Storage in 3D Macroporous Ge@C Composite

*Jianxiu Cheng, Jiaqing Wang, Weihan Li, Xiaowu Liu, Yan Yu**

Abstract

Porous Ge@C composite was synthesized by magnesiothermic reduction reaction of GeO_2，Mg powers and glucose followed by an etching process with HCl solution. Compared to porous Ge electrode, the porous Ge@C composite electrode delivers better cycling stability (~100% capacity retention after 100 cycles at the 0.2 C rate) and higher rate capability (440 $mAhg^{-1}$ at 1800 mAg^{-1}). The improved electrochemical performance results from the synergistic effect of 3D interconnected porous structure and carbon shells. The local pore could buffer the volume change and the conductive carbon shell could prevent the aggregation of Ge as well as enhance the electronic conductivity of the whole electrode.

1. Introduction

Lithium-ion batteries (LIBs) are one of the most promising energy storage devices for electric vehicles (EVs) owing to their high power and energy.[1-3] For commercialization of EVs, the electrochemical performance and safety of LIBs still need further improvement, and thus it is essential to develop electrode materials with higher reversible capacity.[4-6] Compared with the traditional graphite anode, which has a theoretical specific capacity of 372 mA h g^{-1}, group IV A materials such as Si，Ge and Sn have been considered as very promising anode materials for LIBs because of their higher theoretical specific capacities (4200 mAh/g for Si, 1600 mAh/g for Ge, and 991 mAh/g for Sn).[7-9] Among these, Ge has attracted much attention because of its excellent lithium-ion diffusivity (400 times faster than in Si), high electrical

* J. Cheng, J. Wang, W. Li, X. Liu, Prof. Y. Yu, CAS Key Laboratory of Materials for Energy Conversion, Department of Materials Science and Engineering, University of Science and Technology of China, Anhui Hefei 230026, P. R. China. E-mail: yanyumse@ustc.edu.cn

conductivity (~100 times higher than Si), and higher theoretical specific capacity.[10-14] However, the practical application of Ge anode has thus been mainly prevented by the enormous volume change (300–400%) experienced during the lithiation/delithiation process, which results in more capacity losses due to increased solid electrolyte interphase (SEI) formation while delamination results in loss of electrical contact with the current collector. [12,15] To mitigate the above-mentioned challenges and improve the cyclability of Ge anode, much effort has been made to minimize such volume strain during Li-Ge alloying/dealloying process, including the use of 0D nanoparticles, 1D nanowires, hollow nanotube, and 3D-porous nanoparticles.[10, 12, 16-26] Another effective approach to improve the capacity retention is to construct Ge–carbon composites (such as Ge nanoparticles on CNT and Ge/C core-shell).[27, 28] Among those morphologies, 3D porous structure with conductive carbon coating has been proven to be most effective in accommodating the volume changes of electrode materials during cycling, because the local void space can buffer the volume change and the carbon coating can prevent the aggregation of active material. For instance, Cho et al. synthesized 3D porous Ge using a template method, which induces a very stable cycling performance (1400 $mAhg^{-1}$ at a rate of 1 C), showing only a 2% capacity decrease after 100 cycles.[17]

Taking advantages offered by both porous nanostructure and conductive carbon coating on the electrode materials, we herein report a carbon coated 3D macroporous Ge (denoted as porous Ge@C) anode material using a facile magnesiothermic reduction reaction of GeO_2, Mg and glucose under Ar/H_2 atmosphere in an open crucible.[29, 30] To demonstrate the improvement of electrochemical performance of 3D porous Ge@C, we also prepared porous Ge and carbon coated Ge partciles (denoted as Ge@C) as anode materials for LIBs, respectively. The obtained porous Ge@C composite shows the best electrochemical performance and delivers 776mAh/g after 100 cycles at 0.2C. When cycled at a current density of 1800 mA/g, it still displays a reversible capacity as high as ~500 mAh/g. This specific 3D porous structure plays an important role in optimizing electrochemical performance of the Ge anode. Firstly, the 3D porous structure offers enough void space to buffer the volume change and

prevent electronic isolation after long life cycle; Secondly, the uniform surface conductive carbon coating provides electron percolation paths from the current collector to the active particles (3D porous Ge); Thirdly, the carbon coating layer could effective prevent the aggregation of Ge during alloying/dealloying process.

2. Experimental

2.1 Synthesis of porous Ge@C composite, Ge@C composite and porous Ge

The porous Ge@C composite was synthesized by a facile magnesiothermic reduction reaction under Ar/H_2 atmosphere. In a typical procedure, 0.3g germanium dioxide (99.9%, Sigma Aldrich)，0.2g Mg power (99%, Sigma Aldrich,-325mesh) and 0.25g glucose (99.9%, Sigma Aldrich) were mixed completely and ground to get a uniform gray mixture in the glove box filled with Ar. The obtained mixture then was heated in a tube furnace at 650℃ for 4h under Ar (95 v%)/H_2 (5 v%) atmosphere. The heating rate was kept at 3℃/min. The obtained black power was immersed by 1M HCl solution and ultrasound one hour to remove MgO. Then the power was washed with ethanol and dried at 70 ℃ in a vacuum oven for 12h. For comparison，0.3g germanium dioxide and 0.2g Mg power were mixed and ground, then the gray powder was heated at 650℃ to get pure porous Ge powder. Germanium dioxide and glucose were groundand then were heated to get Ge@C composite.

2.2 Characterization techniques

The structure and morphology of the obtained samples was characterized by X-ray diffraction (XRD, Philips X'Pert Pro Cu K_α radiation), Field-emission scanning electron microscopy (FESEM, JEOL, Tokyo, Japan) and High-resolution transmission electron microscopy (HETEM, JEOL 4000EX Tokyo, Japan). The thermogravimetric differential thermal analysis of porous Ge@C power was conducted with a thermogravimetry differential thermal analyzer (Shi-madzu, TGA-50) under air atmosphere with a heating rate of 10℃/min from room temperature to 1000℃.

2.3 Electrochemical measurements

Electrochemical measurements were performed using LIR2032 coin-type cells assembled in glove box filled with Ar. The active material, (porous Ge@C composite, Ge@C composite or porous Ge powers) carbon black and PVDF were mixed in a

mass ratio of 75:15:10. The resultant slurry was then uniformly coated on a Cu foil current collector and dried at 80℃ in vacuum oven. Electrochemical cells were assembled with porous Ge@C composite, Ge@C composite or porous Ge electrode，metallic lithium foil as counter electrode and Celgard 2400 as separator. The weight of each piece of electrode is around 2 mg. The electrolyte was a solution of 1 M $LiPF_6$ in ethylene carbonate and diethyl carbonate (EC: DEC=1:1,v/v). The cells were charged and discharged galvanostatically in the fixed voltage window from 5 mV to 1.5 V on a Neware battery tester at room temperature.

3. Results and discussion

Fig. 1a shows the XRD patterns of the porous Ge@C composite, Ge@C composite and porous Ge, in which all peaks are in agreement with pure Ge (JCPDS card no.04-0545). No GeO_2 or MgO peaks were detected, indicating the impurity phases were totally removed after washing with HCl. The absence peak of carbon in the XRD patterns of porous Ge@C composite implies that the carbon is not well crystallized. The (002) peak of porous Ge@C at 27.3° that is very close to (002) peak of graphite (27°), which may be attribute to a more graphitic carbon coating layer formation after heating in Ar/H_2 atmosphere. Fig.1b presents the TGA-DSC profiles of the porous Ge@C, performed inflowing air with a heating rate of 10℃/min. A sharp exothermic peak of DSC curve centered at 580℃ is observed, which corresponds to the oxidation of Ge to GeO_2. The weight loss at around 800℃ is caused by carbon combustion reaction. TGA curve shows that the carbon and Ge weight contents are approximate 23 wt% and 77 wt%, respectively. The TGA-DSC profiles of Ge@C composite have the same result. Further structural information is provided by the Raman spectra in Fig.1(c). Appearance of a strong Raman peak located at 298cm^{-1} in porous Ge confirms the well crystalline Ge. In case of porous Ge@C composite and Ge@C composite, the intensity of Ge declines and the D and G band of C appears which proves that C has a certain proportion in composite. The ordering of carbon in the composite can also be seen in Raman spectra. The intensity ratio of the D band to the G band is 1.02:1 in porous Ge@C composite (red line) and 1.08:1 in Ge@C composite (blue line), which also indicated the formation of a

disordered carbon structure. In case of Ge@C composite, the degree of disordering of carbon is higher than that of porous Ge@C composite.

SEM images (Fig. 2) reveal the structure of porous Ge, porous Ge@C composite and Ge@C composite synthesized by GeO_2 and glucose. The particles of porous Ge (Fig. 2a), with a size of around 5μm, exhibit a coherent macroscopic network structure with a pore size distribution ranging from 200 nm to 600 nm in diameter. Fig .2b shows the wall thickness of pores ranges from 150 to 250 nm. When the precursor materials contain glucose，the obtained porous Ge@C composite (Fig. 2c) displays similar porous structure with the pure porous Ge powder. The pore size decreases to 100~200nm, which attributes to the carbon partially fill in the interconnecting macropores of Ge and conform coat on the Ge surface. When GeO_2 was reacted directly with glucose, the product presents block structure (Fig.2e&2f) and the shape of particles is extremely irregular. This proves that the appearance of pores in porous Ge@C composite is due to the participation of magnesium powder.

The 3D interconnected porous structure of the Ge@C composite and Ge powder are further confirmed by the transmission electron microscopy (TEM) micrograph (Fig. 3a &3c). The High-resolution transmission electron microscopy (HRTEM) (Fig.3b) reveals that the porous Ge powder have a diamond cubic structure. After coated with carbon, the Ge remains the cubic structure, where crystalline planes of Ge (220) with a distance spacing of 0.2 nm can be clearly observed. It can also clearly be seen that the porous Ge are well-covered by a carbon layer with a thickness of 4 nm (Fig. 3d). For Ge@C composite (Fig. 3e &3f), the distribution of Ge and C is not uniform compared with the porous Ge@C composite. Furthermore, the distance of the crystalline planes of Ge becomes larger.

Figure 4a, 4b & 4c display the galvanostatic discharge-charge voltage profiles and cycling performance of porous Ge, porous Ge@C composite and Ge@C composite at 0.2C ($320mAg^{-1}$) in the voltage range of 0.005-1.5V, respectively. Two plateaus (Fig. 4a) were observed at 0.2V and 0.4 V during the first discharge process, which can be related to the alloying of Li with Ge.[32] The first discharge and charge capacities are 1738 and 1073 $mAhg^{-1}$ for the porous Ge powder, with an initial

Coulombic efficiency (CE) of 61%. The large capacity loss is most likely attributed to formation of SEI layer on the electrode surface during the first discharge step.[31, 32] In case of porous Ge@C composite (Fig. 4b), it delivers a capacity of 1821 and 981 $mAhg^{-1}$ for 1st discharge and charge, respectively, corresponding an initial CE of 53.9%. The higher initial capacity loss of porous Ge@C composite than that of Ge powder may be result from enhanced formation of SEI layers on the porous Ge@C composite surface during the first cycles.[33, 34] After the first cycle, the CE of porous Ge@C composite electrode was significantly improved to 99% for up to 100 cycles. For Ge@C composite (Fig. 4c), it shows a capacity of 1763 and 852 $mAhg^{-1}$ for the first discharge and charge, respectively, with an initial CE of 48.3%. In the following cycles, the capacity decreased rapidly, indicting lower capacity retention of Ge@C composite.

Fig.4d shows the capacity retention of porous Ge, porous Ge@C composite and Ge@C composite electrodes at 0.2C. The capacity of Ge@C composite decreases rapidly after two cycles because that there are no pores to sustain the large volume change during discharge and charge processes. Both porous Ge and porous Ge@C composite powder delivers similar capacity in the first 20 cycles. The capacity of porous Ge powder degrades rapidly afterwards result from the large volume change (>300%) during lithium alloying/dealloying processes, leading to an electrical disconnection between particles. In contrast, porous Ge@C composite electrode shows a significantly improved cyclability. It could be attributed to the special carbon coated porous structure, which confined a variety of advantages: offering sufficient void space to accommodate the large volume change, providing an interconnected electron and ion transfer path during the long cycle life, preventing cracking as well as morphology stability. The porous Ge@C composite electrode still delivers a reversible capacity of ~790 $mAhg^{-1}$ after 100 cycles at 0.2C, which is ~2 times higher than that of the theoretical capacity of graphite. Furthermore, as shown in Fig. 4e, the porous Ge@C composite electrode also shows a better rate capability than porous Ge electrode and Ge@C composite at the same current density. The porous Ge@C composite electrode delivers reversible capacities of 590, 530, and 440

$mAhg^{-1}$ at 600, 900, and 1800 mAg^{-1}, respectively. Note that after cycled at high C rate, the electrode can recover and delivers a reversible capacity as high as 1015 $mAhg^{-1}$ when the current density was tuned back to 100 mAg^{-1}, implying its good reversibility. In case of porous Ge electrode, it only delivers capacities of 300, 180, and 50 $mAhg^{-1}$ at the same current density. And for Ge@C composite, it only displays reversible capacities of 20, 12, and11 $mAhg^{-1}$ at the same current density, respectively. Notably, the discharge capacity of both porous Ge@C and porous Ge at higher current density (320mA/g in Fig.4c) are better than those obtained from the stepwise cycling starting from 100mA/g (Fig4e). It could be attributed to the interfacial storage of lithium, which has been demonstrated in mesoporous TiO_2 anode.[35]

4. Conclusions

In conclusion, we have successfully fabricated porous Ge@C composite via magnesiothermic reduction reaction of GeO_2, Mg and glucose. The porous Ge@C composite exhibits a coherent macroscopic network structure with a pore size distribution ranging from 200 nm to 600 nm in diameter and a uniform carbon coated layer (~4nm) on the surface. As an anode material for LIBs, the porous Ge@C composite exhibits excellent cycling performance and improved rate capability in comparison with porous Ge electrode, which attributes to the synergistic effect of 3D interconnected porous structure and conducting carbon shell. The local pore could buffer the volume change and the conductive carbon shell could prevent the aggregation of Ge as well as enhance the electronic conductivity of the whole electrode. This porous Ge@C composite can be considered as a promising anode material for LIBs.

Acknowledgements

This work was supported by the National Natural Science Foundation of China (No.21171015, No. 21373195) ， the Recruitment Program of Global Experts, program for New Century Excellent Talents in University (NCET), the Fundamental Research Funds for the Central Universities (WK2060140014, WK2060140016).

References:

1. Ji, L.; Lin, Z.; Alcoutlabi, M.; Zhang, X. *Energy & Environmental Science* **2011,** 4, (8), 2682.
2. Yuan, F.-W.; Yang, H.-J.; Tuan, H.-Y. *ACS NANO* **2012,** 6, (11), 9932-9942.
3. Ren, J.-G.; Wu, Q.-H.; Tang, H.; Hong, G.; Zhang, W.; Lee, S.-T. *Journal of Materials Chemistry A* **2013,** 1, (5), 1821.
4. Baggetto, L.; Notten, P. H. L. *J Electrochem Soc* **2009,** 156, (3), A169-A175.
5. Yu, Y.; Gu, L.; Wang, C.; Dhanabalan, A.; van Aken, P. A.; Maier, J. *Angewandte Chemie* **2009,** 48, (35), 6485-9.
6. Tan, L. P.; Lu, Z.; Tan, H. T.; Zhu, J.; Rui, X.; Yan, Q.; Hng, H. H. *J Power Sources* **2012,** 206, 253-258.
7. T.Lee, K.; C.Lytle, J.; S.Ergang, N.; M.Oh, S.; Stein, A. *Advanced Functional Materials* **2005,** 15, (4), 547-556.
8. Hwa, Y.; Park, C.-M.; Yoon, S.; Sohn, H.-J. *Electrochim Acta* **2010,** 55, (9), 3324-3329.
9. Song, T.; Jeon, Y.; Samal, M.; Han, H.; Park, H.; Ha, J.; Yi, D. K.; Choi, J.-M.; Chang, H.; Choi, Y.-M.; Paik, U. *Energy & Environmental Science* **2012,** 5, (10), 9028.
10. Kim, M. G.; Cho, J. *J. Electrochem. Soc.* **2009,** 156, (4), A277-A282.
11. Graetz, J.; Ahn, C. C.; Yazami, R.; Fultz, B. *Electrochemical and Solid-State Letters* **2003,** 6, (9), A194-A197.
12. Cui, G.; Gu, L.; Zhi, L.; Kaskhedikar, N.; van Aken, P. A.; Müllen, K.; Maier, J. *Adv. Mater.* **2008,** 20, (16), 3079-3083.
13. Yoon, S.; Park, C.-M.; Sohn, H.-J. *Electrochemical and Solid-State Letters* **2008,** 11, (4), A42.
14. Xue, D. J.; Xin, S.; Yan, Y.; Jiang, K. C.; Yin, Y. X.; Guo, Y. G.; Wan, L. J. *J Am Chem Soc* **2012,** 134, (5), 2512-5.
15. Chan, C. K.; Zhang, X. F.; Cui, Y. *Nano letters* **2008,** 8, (1), 307-309.
16. Park, M. H.; Cho, Y.; Kim, K.; Kim, J.; Liu, M.; Cho, J. *Angewandte Chemie* **2011,** 50, (41), 9647-50.
17. Park, M. H.; Kim, K.; Kim, J.; Cho, J. *Adv Mater* **2010,** 22, (3), 415-8.
18. Seo, M.-H.; Park, M.; Lee, K. T.; Kim, K.; Kim, J.; Cho, J. *Energy & Environmental Science* **2011,** 4, (2), 425.
19. Lee, H.; Kim, M. G.; Choi, C. H.; Yang-Kook, S.; Yoon, C. S.; Cho, J. *Journal of physical Chemistry B* **2005,** 109, (44), 20719-20723.
20. Park, C.-M.; Sohn, H.-J. *Journal of Chemical Materials* **2008,** 20, (9), 3169-3173.
21. Graetz, J.; Ahn, C. C.; Yazami, R.; Fultz, B. *Electrochemical and Solid-State Letters* **2003,** 6, (9), A194.
22. Sandu, I.; Moreau, P.; Guyomard, D.; Brousse, T.; Roue, L. *Solid State Ionics* **2007,** 178, (21-22), 1297-1303.
23. Obrovac, M. N.; Christensen, L.; Le, D. B.; Dahn, J. R. *J Electrochem Soc* **2007,** 154, (9), A849.

24. Kim, J.-H.; Kim, H.; Sohn, H.-J. *Electrochemistry Communications* **2005,** 7, (5), 557-561.
25. Saint, J.; Morcrette, M.; Larcher, D.; Laffont, L.; Beattie, S.; Pérès, J. P.; Talaga, D.; Couzi, M.; Tarascon, J. M. *Advanced Functional Materials* **2007,** 17, (11), 1765-1774.
26. Cui, G.; Gu, L.; Zhi, L.; Kaskhedikar, N.; van Aken, P. A.; Müllen, K.; Maier, J. *Adv Mater* **2008,** 20, (16), 3079-3083.
27. Hwang, I.-S.; Kim, J.-C.; Seo, S.-D.; Lee, S.; Lee, J.-H.; Kim, D.-W. *Chemical Communications* **2012,** 48, (56), 7061-7063.
28. Seng, K. H.; Park, M. H.; Guo, Z. P.; Liu, H. K.; Cho, J. *Angewandte Chemie-International Edition* **2012,** 51, (23), 5657-5661.
29. Bao, Z. H.; Weatherspoon, M. R.; Shian, S.; Cai, Y.; Graham, P. D.; Allan, S. M.; Ahmad, G.; Dickerson, M. B.; Church, B. C.; Kang, Z. T.; Abernathy, H. W.; Summers, C. J.; Liu, M. L.; Sandhage, K. H. *Nature* **2007,** 446, (7132), 172-175.
30. Yu, Y.; Gu, L.; Zhu, C.; Tsukimoto, S.; van Aken, P. A.; Maier, J. *Adv Mater* **2010,** 22, (20), 2247-+.
31. Kim, H.; Seo, M.; Park, M.-H.; Cho, J. *Angewandte Chemie International Edition* **2010,** 49, (12), 2146-2149.
32. Yu, Y.; Yan, C.; Gu, L.; Lang, X.; Tang, K.; Zhang, L.; Hou, Y.; Wang, Z.; Chen, M. W.; Schmidt, O. G.; Maier, J. *Advanced Energy Materials* **2013,** 3, (3), 281-285.
33. Yang, L. C.; Gao, Q. S.; Li, L.; Tang, Y.; Wu, Y. P. *Electrochemistry Communications* **2010,** 12, (3), 418-421.
34. Yin, Y.-X.; Xin, S.; Wan, L.-J.; Li, C.-J.; Guo, Y.-G. *The Journal of Physical Chemistry C* **2011,** 115, (29), 14148-14154.
35. Shin J.-Y, Samuelis D., Maier J., *Adv. Funct. Mater.* **2011**, 21, 3464-3472.

Figure Captions:

Fig. 1a XRD patterns of porous Ge, porous Ge@C composite and Ge@C composite. The peak positions and intensities for cubic phase Ge are marked in the XRD. (JCPDS No.04–0545). The inset image is the magnified XRD patterns of porous Ge@C composite and Ge@C composite from 27^{o} to 27.5^{o}.

Fig. 1b TGA-DSC curves of porous Ge@C composite. Heat rate is 10 ^{o}C/min.

Fig.1c Raman spectra of porous Ge , porous Ge@C composite and Ge@C composite.

Fig. 2 SEM image (a) and FESEM image (b) of porous Ge. SEM image (c) and FESEM image (d) of porous Ge@C composite. SEM image (e) and (f) of Ge@C composite.

Fig. 3 TEM image (a) and HRTEM image (b) of porous Ge. TEM image (c) and HRTEM image (d) of porous Ge@C composite.TEM image (e) and HRTEM image (f) of Ge@C composite.

Fig. 4 Electrochemical performance of porous Ge, porous Ge@C composite and Ge@C composite electrodes cycled between 0.005 V and 1.5 V vs. Li^{+}/Li. Voltage profiles of the porous Ge electrode (a), porous Ge@C composite electrode (b) and Ge@C composite electrode (c) at a cycling rate of 0.2 C, the cycle numbers were marked in the picture; (d)capacity retention of porous Ge, porous Ge@C composite and Ge@C composite electrodes at 0.2C rate. (e)Rate capability of porous Ge ,porous Ge@C composite and Ge@C composite electrodes. (The current density was marked in the picture).

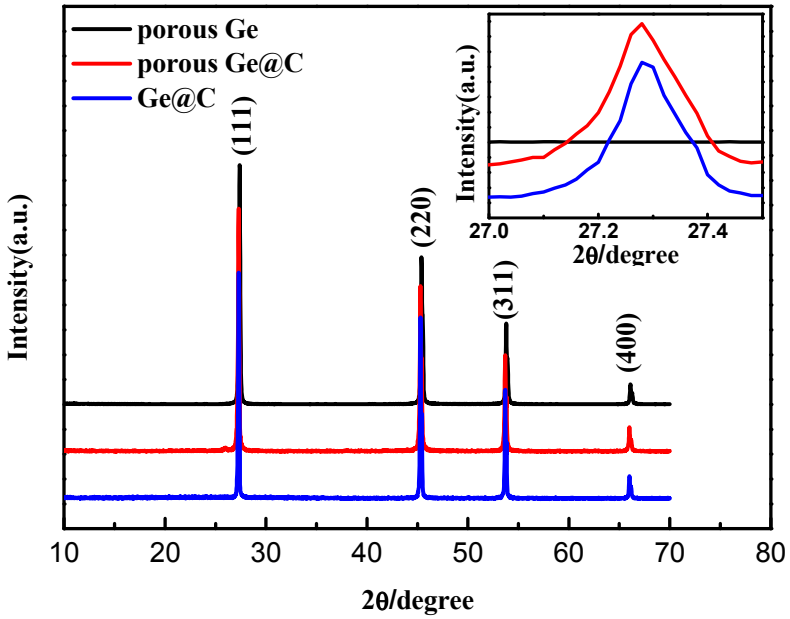

Fig.1a

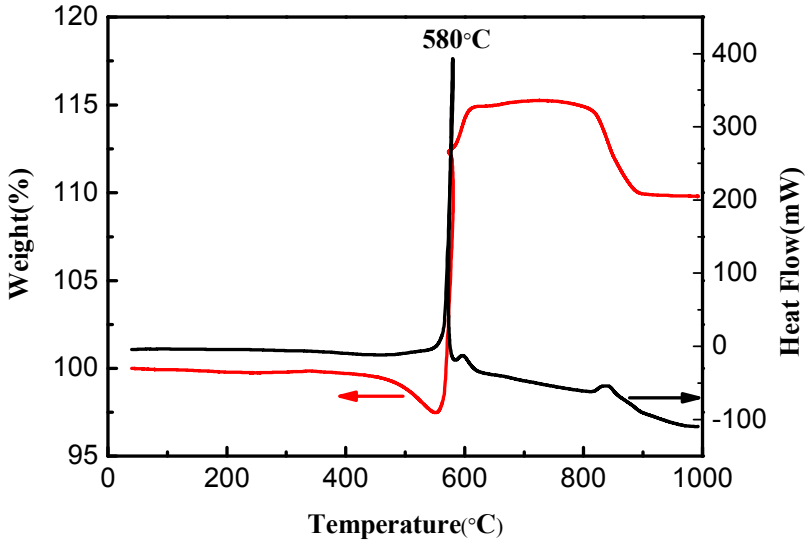

Fig.1b

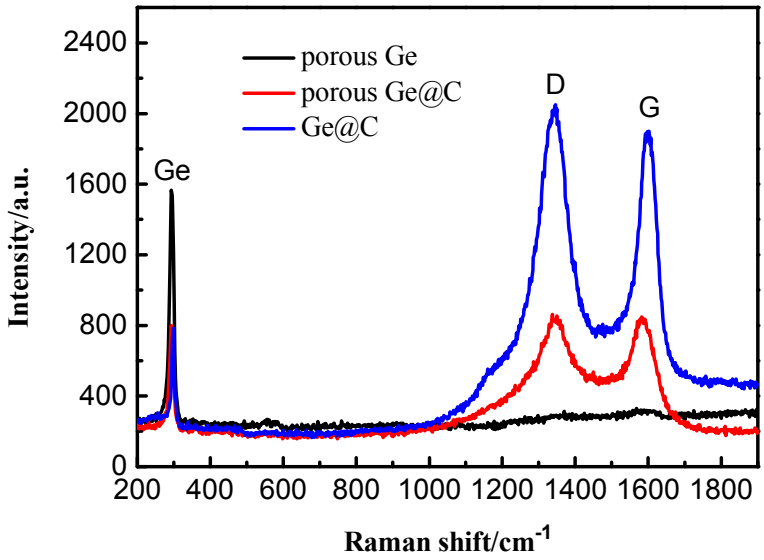

Fig.1c

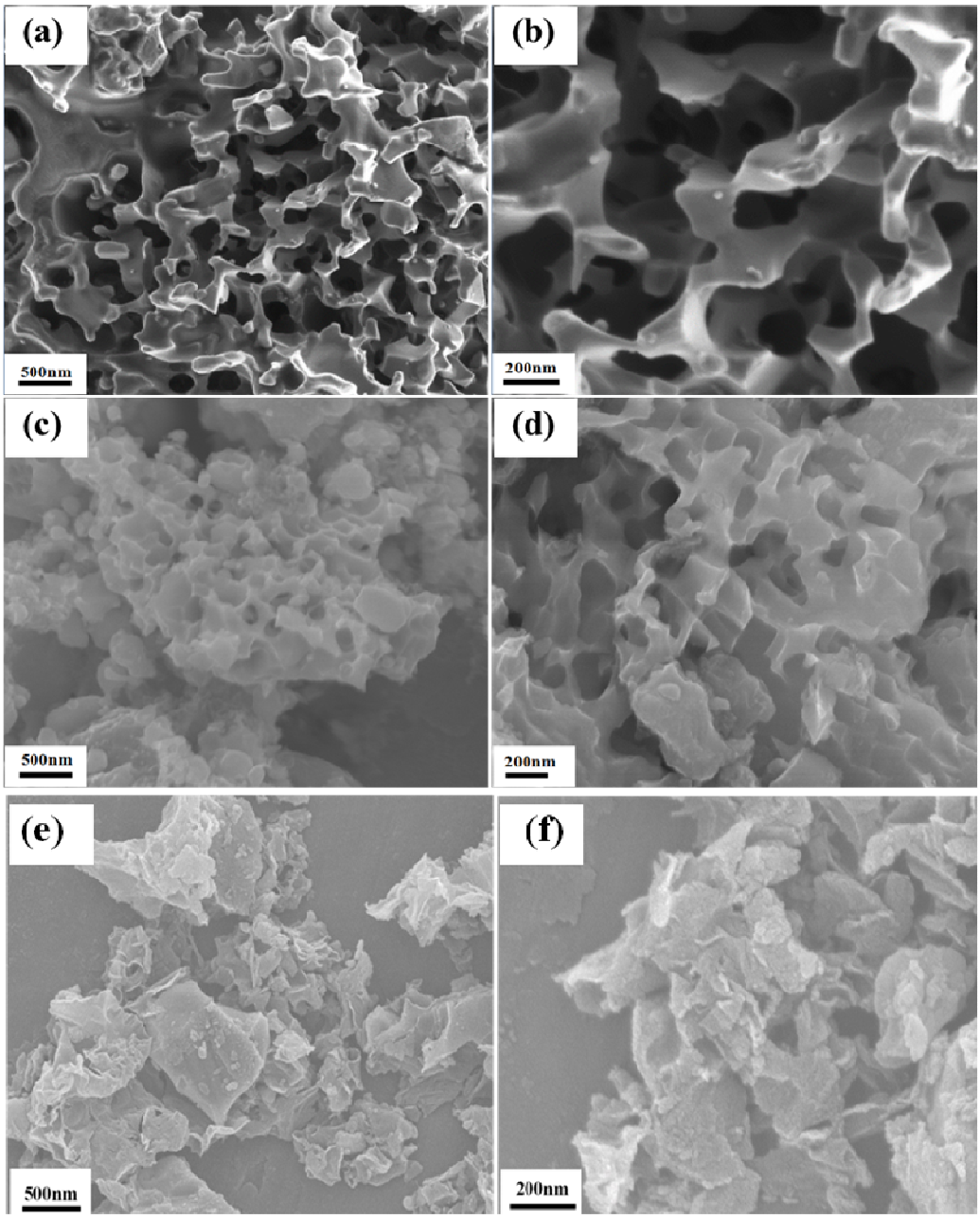

Fig. 2

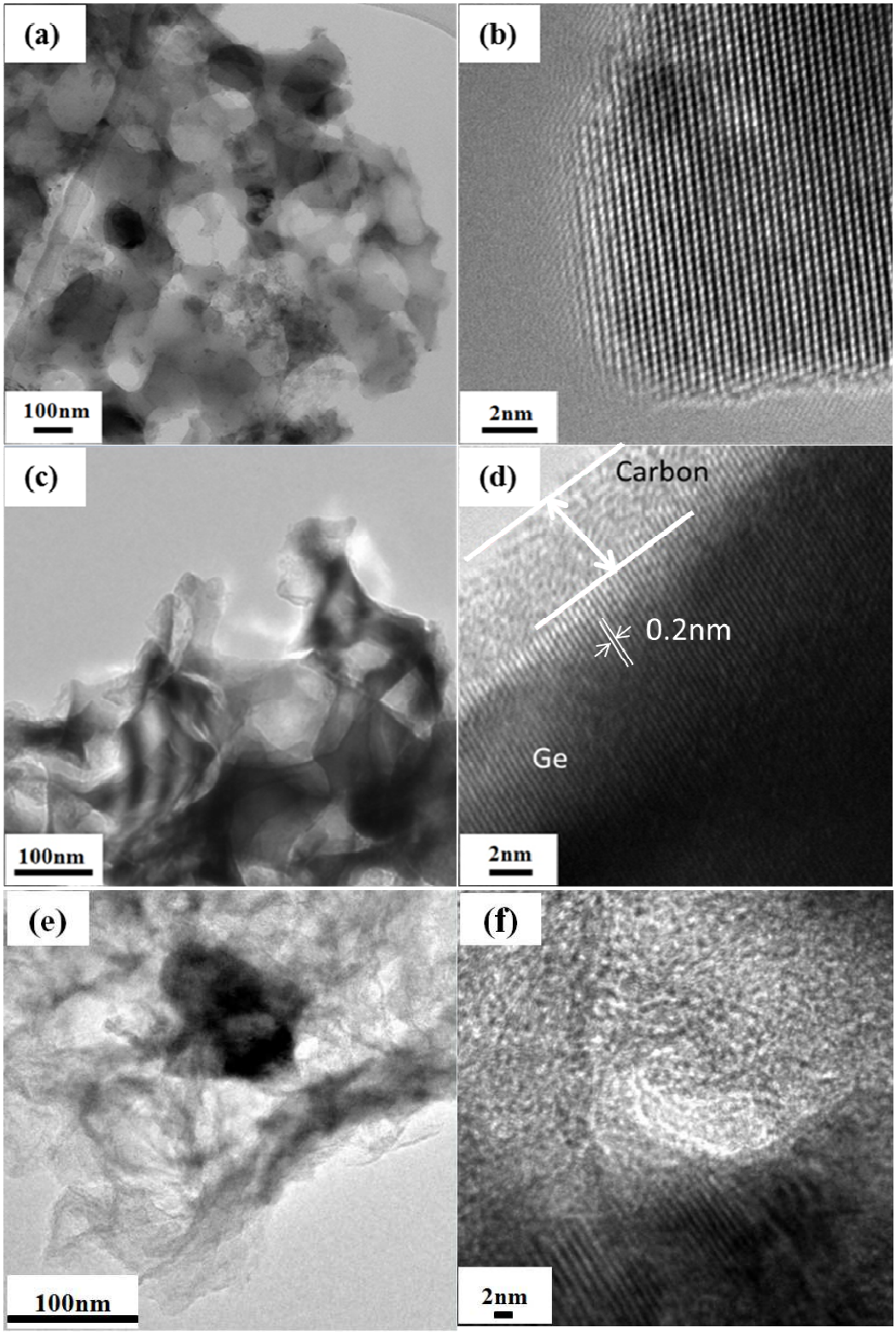

Fig.3

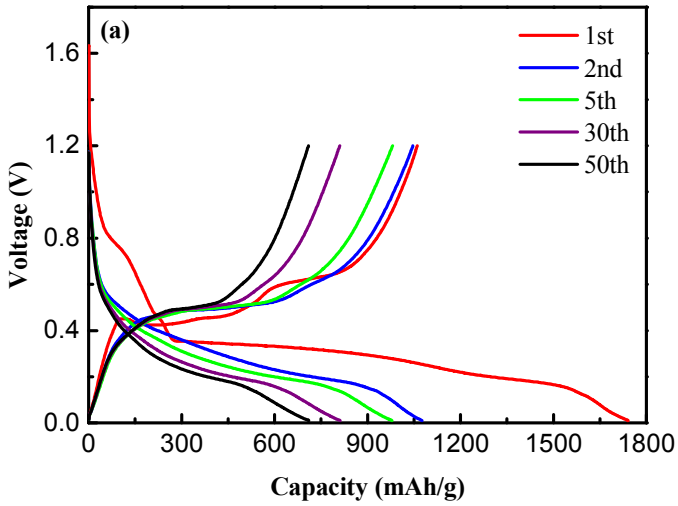

Fig.4a

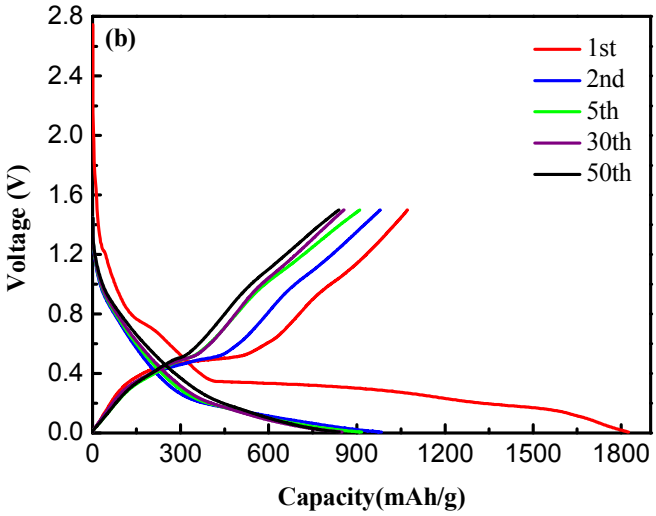

Fig.4b

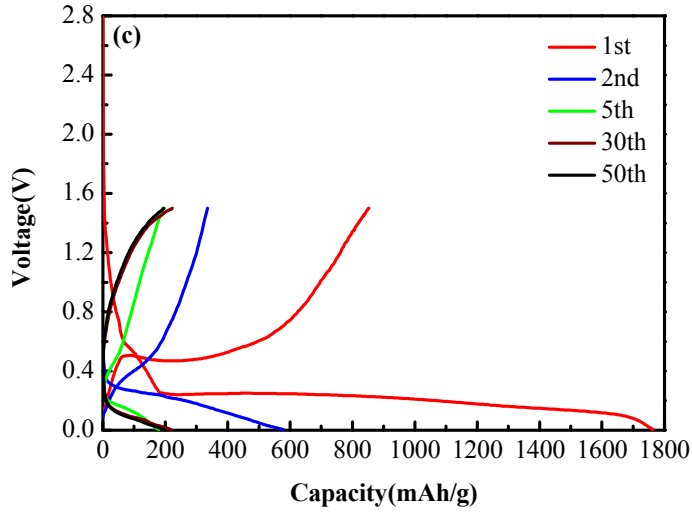

Fig.4c

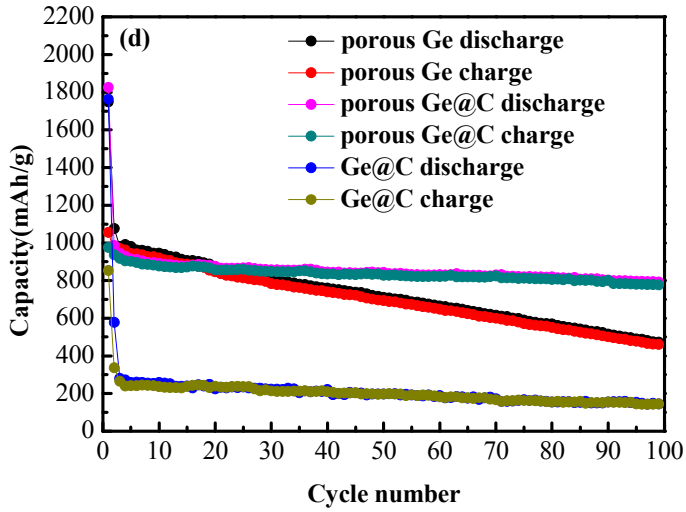

Fig.4d

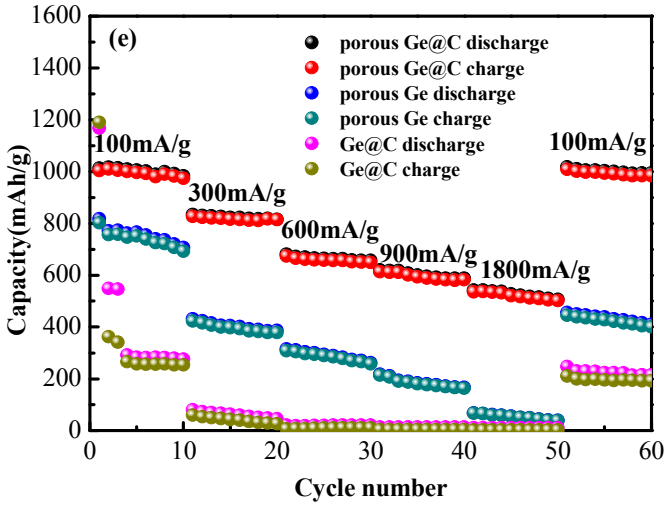

Fig.4e